In situ study of hydride precipitation kinetics and re-orientation in Zircaloy using synchrotron radiation

K.B. Colas [a,*], A.T. Motta [a], J.D. Almer [b], M.R. Daymond [c], M. Kerr [c], A.D. Banchik [d], P. Vizcaino [d], J.R. Santisteban [e]

[a] *Department of Mechanical and Nuclear Engineering, Penn State University, University Park, PA, USA*
[b] *Advanced Photon Source, Argonne National Laboratory, Argonne, IL, USA*
[c] *Department of Mechanical and Materials Engineering, Queen's University, Kingston, ON, Canada*
[d] *CNEA, Buenos Aires, Argentina*
[e] *CONICET and Instituto Balseiro, Centro Atomico Bariloche, Argentina*

Abstract

The orientation and distribution of hydrides formed in zirconium alloy nuclear fuel cladding can strongly influence material behavior and in particular resistance to crack growth. The hydride microstructure and hydride platelet orientation (whether in-plane or radial relative to the cladding tubes) are crucial to determining cladding failure limits during mechanical testing. Hydride formation is normally studied by post-facto metallography, performed at room temperature and in the absence of applied stress. This study uses synchrotron radiation to observe in situ the kinetics of hydride dissolution and precipitation in previously hydrided Zircaloy samples. The experiments allow the direct observation of hydride dissolution, re-precipitation, and re-orientation, during heating and cooling under load. The solubility limits and the hydride-matrix orientation relationship determined from in situ experiments were in good agreement with previous post-facto examinations of bulk materials. The present measurements performed under stress and at temperature showed a characteristic diffraction signature of reoriented hydrides. The results suggest a threshold stress for hydride re-orientation between 75 and 80 MPa for the microstructure/texture studied. These results are discussed in light of existing knowledge.
© 2010 Acta Materialia Inc. Published by Elsevier Ltd. All rights reserved.

Keywords: Synchrotron radiation; Hydride; Zirconium alloys; Hydride re-orientation

1. Introduction

Zirconium alloys are used in the nuclear industry worldwide for nuclear fuel cladding because their combination of low neutron capture cross-section, good mechanical properties, and corrosion resistance makes them uniquely suited for in-reactor applications. In light water reactors (LWRs) hydrogen ingress occurs during waterside corrosion of the zirconium alloy cladding of the nuclear fuel rods. For high burn-up fuel, oxide thicknesses up to 100 μm and hydrogen content in excess of 700 wt. ppm have been observed [5]. This hydrogen uptake is detrimental to fuel cladding performance [1,2]. This is because the solubility of hydrogen in zirconium is low (below 10 wt. ppm at room temperature [4]) and brittle zirconium hydride phases form, which can degrade the cladding mechanical properties [6].

The hydrides observed in fuel cladding exposed to reactor environment are most often fcc delta hydrides ZrH_x (where $x \sim 1.6$) [7] although gamma and epsilon hydrides are occasionally observed [8,9]. Delta hydrides are shown by electron microscopy to be platelet-shaped and to form with a near $(1\,1\,1)_\delta //(0\,0\,0\,2)_\alpha$ orientation relationship with the alpha zirconium matrix [10]. The larger macroscopic hydride plates observed optically have been reported to be constituted of a stacking of several of these

---

* Corresponding author. Address: 18 Reber Building, Department of Mechanical and Nuclear Engineering, Penn State University, University Park, PA 16802, USA. Tel.: +1 814 865 9709; fax: +1 814 865 8499.
E-mail address: kuc147@psu.edu (K.B. Colas).

microscopic platelets [11]. The orientation and morphology of these macroscopic hydrides are primarily dependent on the zirconium matrix microstructure, thermal history and stress state (both applied and residual). In the absence of a stress field, hydride precipitation is dependent on the texture of the zirconium matrix and is governed by the orientation of the last compressive step in the thermo-mechanical treatment [12]. The presence of a sufficiently high applied stress field causes the hydride platelets to precipitate preferentially perpendicular to the applied stress direction. The level of applied stress required for hydride re-orientation is dependent on the microstructure and prior processing [13]. Because of this, concern has arisen that hydride re-orientation (by dissolution and re-precipitation under load) could occur during temperature and loading cycles during dry storage of spent fuel, which would cause the fuel cladding to become more brittle. As a result, understanding of hydride re-orientation is of great technological importance.

Most analyses of hydride microstructural changes have been performed post-facto, at room temperature and under no applied stress. In many of these analyses, the hydride orientation is measured on metallographs before and after heating and loading cycles [14–16]. These studies show that re-orientation of hydrides is dependent on the stress intensity and direction, the zirconium matrix texture, the initial stress state of the materials and the cooling rates. It would be of great interest to combine post-facto metallographic techniques with in situ measurements of hydride re-orientation. Recent studies using high energy synchrotron X-rays have demonstrated that it is possible to observe zirconium hydride phases and distinguish the crystallographic nature of the hydride phases present (delta from gamma for example) at low hydrogen concentrations [3]. Strain measurements of zirconium hydrides embedded in a zirconium alloy matrix have been conduced both in the bulk and at notch tips [17,18]. Zirconium hydride precipitation and dissolution have also been studied using neutron diffraction [19,20]. This technique allows in situ measurements of hydride diffracted intensities, thus allowing to determine the influence of heating and cooling rates on the relative volume fractions of the delta and gamma phases. However neutron diffraction requires very long holding times at temperature (on the order of 1 or 2 h) for the diffraction patterns of such small volume fraction minority phases to be recorded and therefore changes in hydride phase can only be monitored over relatively long time scales.

The aim of this study is to present an in situ technique for observation of hydride dissolution and precipitation in zirconium alloys. The use of synchrotron radiation from the Advanced Photon Source (APS) at Argonne National Laboratory allows examination of hydride diffraction peaks in situ with good angular resolution. The beamline utilized has high energy X-rays allowing transmission experiments to be performed, and is equipped with load cells and a furnace. These techniques were used to observe hydride re-orientation in the matrix of zirconium alloys during heating and cooling cycles under stress.

2. Experimental procedures

Both Zircaloy-2 and Zircaloy-4 samples were used in this study. Zircaloy-2 samples were taken from a warm-rolled and fully recrystallized square bar of 60 mm × 60 mm. The samples were cut from the center of the square bar to minimize deformation and/or texture inhomogeneities. Optical examination of the microstructure of the samples both before and after hydriding revealed a relatively homogeneous microstructure of the matrix and the hydrides. The samples exhibit an equiaxed zirconium grain structure with an average diameter of 20 μm. Zircaloy-4 was furnished by Western Zirconium in the form of a 0.5 mm thick sheet in the cold-rolled stress relieved condition. As a result the grains are not equiaxed, but elongated in the rolling direction. The Zircaloy-2 material used in this study was well characterized in terms of texture/mechanical properties, as discussed below [21]. The crystallographic texture of the Zircaloy-2 was obtained by neutron diffraction and the {0 0 0 2} and {1 0 $\bar{1}$ 0} pole figures are shown in Fig. 1. The {0 0 0 2} pole figure shows a strong normal texture, with the basal poles are concentrated near the normal direction to rolling, with some intensity along the transverse direction and little intensity in the rolling direction. Quantitatively the basal pole texture was assessed by calculating the associated Kearns factors [13], $f_N = 0.887$, $f_T = 0.101$ and $f_R = 0.012$ indicating a stronger basal pole texture than that of common Zircaloy tubing [13]. The sample directions are represented in Fig. 2a, while the testing sample geometry is shown in Fig. 2b. The Zircaloy-4 sheet texture was not measured for this study but it is expected that this will be the typical texture obtained for cold-rolled stress relieved sheet as illustrated in [22].

These samples were hydrogen-charged by high temperature gas diffusion, performed in several steps. First, the native oxide layer present on the surface of the samples
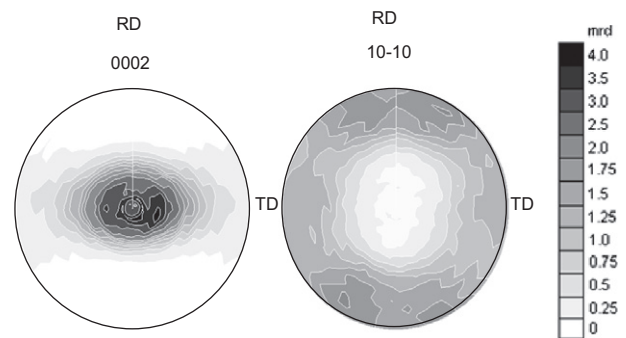
Normal Direction at center, Rolling Direction at 12 o'clock

Fig. 1. Basal {0 0 0 2} and prismatic {1 0 $\bar{1}$ 0} pole figures for Zircaloy-2 plate. The intensity scale is shown on the right [21].
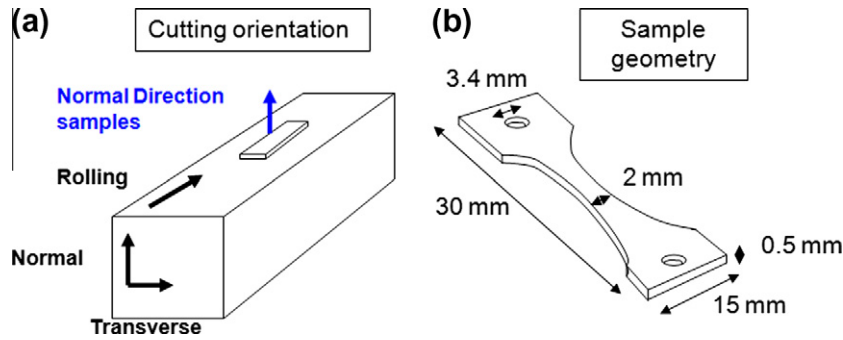
Fig. 2. (a) Material directions and sample cutting orientation and (b) mechanical testing sample geometry.

was removed by dipping the samples for 1 min in an acid solution of one part HF, 10 parts nitric acid and 10 parts H_2O. Second, using an electron-beam evaporator a thin layer of nickel was deposited onto the sample surface to protect from air [22]. The samples were then hydrogen-charged in a vacuum furnace using a mixture of 12% hydrogen and 88% argon, introduced at 450 °C. Several temperature cycles were necessary to charge to the desired level of hydrogen. The total time at 450 °C was 3 h, so no significant re-crystallization occurred [23]. The final hydrogen contents were measured using hot vacuum extraction, performed by Luvak Inc. For each sample two measurements were performed with an uncertainty of ±10 wt. ppm. Table 1 summarizes the materials used in this study, their original thermo-mechanical treatments, the range of hydrogen contents as well as the initial hydride microstructure.

2.1. Metallography

Metallography was performed to characterize the hydride morphology before and after the experiments. The samples were mounted in epoxy casts and mechanically polished to 1200 grit silicon carbide paper, followed by chemical etching using the same solution used for oxide layer removal. This solution preferentially etched the zirconium hydrides, which allowed their observation using optical microscopy.

2.2. Synchrotron X-ray diffraction

X-ray diffraction examination of the samples was conducted at beamline 1-ID at the Advanced Photon Source at Argonne National Laboratory with the objective of observing the dissolution and precipitation kinetics of zir-

Table 1
Summary of materials used, thermo-mechanical treatments and initial hydride microstructure (ND: normal direction; RD: rolling direction).

Material	Zircaloy-2	Zircaloy-4
Thermo-mechanical treatment	Warm rolled recrystallized	Cold-rolled stress relieved
Original material shape	Square bar 60 mm × 60 mm	Sheet 0.5 mm thick
Cut sample shape	Dog-bone (see Fig. 2b)	Dog-bone (see Fig. 2b)
Hydrogen content (in wt. ppm)	From 80 to 600 (several samples)	∼600
Initial hydride microstructure	80 wt.ppm of hydrogen 600 wt.ppm of hydrogen	600 wt.ppm of hydrogen
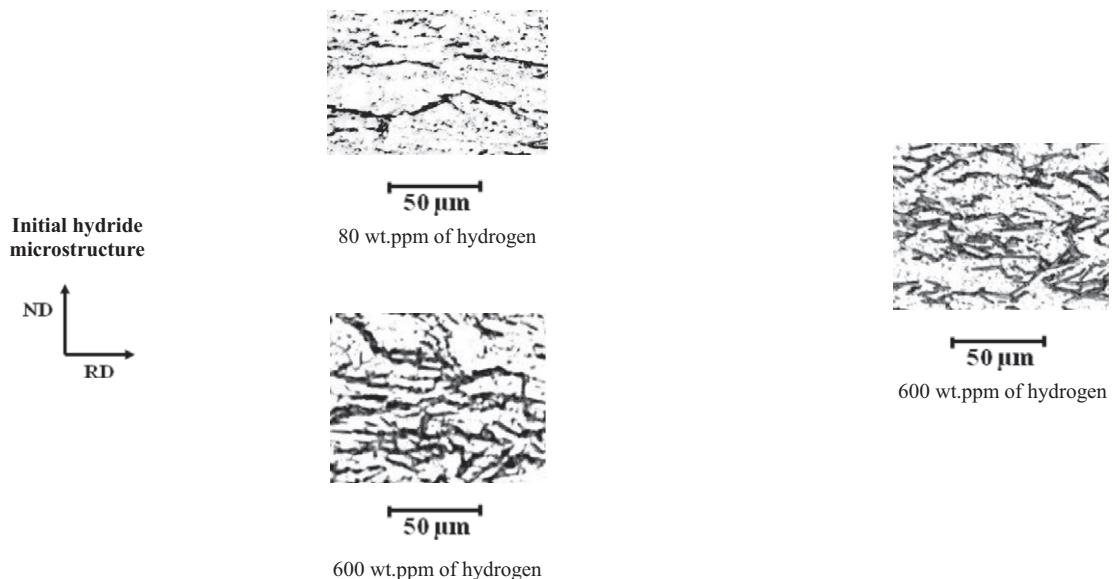
conium hydrides. As illustrated in Fig. 3, the experiments were conducted in transmission geometry, using 80 keV X-rays ($\lambda = 0.015$ nm) with a beam size of 0.3 mm × 0.3 mm [24]. The high X-ray intensities available at the beamline allow the observation of the hydride diffracted intensity as the sample is heated or cooled. The load frame allows the application of different stress levels to the samples as the diffraction pattern is being recorded. A high-speed area detector (1 s time resolution) was used to collect diffraction patterns, allowing the full diffraction rings to be recorded. Because the data was obtained in transmission, the diffraction signal is averaged over the full sample thickness. The diffraction rings obtained can be subsequently integrated over different angular ranges to obtain the diffracted intensity from planes oriented in different directions relative to the macroscopic sample directions. A typical Zircaloy-2 diffraction pattern integrated over the full ring is shown in Fig. 4.

For this study it was chosen to integrate the diffraction rings around specific orientations close to the rolling direction (RD) and transverse direction (TD) as illustrated in Fig. 3. Diffraction signals seen in the 'TD' come from crystallographic planes which have their normals parallel to the TD and diffraction signals in the 'RD' come from crystallographic planes which have their normals parallel to the RD. The samples were placed in an MTS® frame which allowed computer monitoring of the applied force and the displacement, or the displacement rate. The testing temperature was controlled using an optical furnace and the sample temperature was monitored using K-type thermocouples, spot welded onto the sample surface.

The typical raw data obtained during this experiment was in the form of 10 successive 1 s exposure two-dimensional images from the plate detector for each diffraction pattern recorded (this was necessary to avoid detector saturation). The 10 images were summed and averaged by a Matlab® routine [25] and the background was subtracted to obtain the full diffraction rings. Using the Matlab® routine, the full diffraction rings were integrated over four specific angular ranges of ±10° around 0°, 90°, 180° and 270°. The angular ranges obtained were then averaged (average of the sum of 0° and 180° ranges and average of the sum of 90° and 270° ranges) and reduced to a one dimensional GSAS file (diffracted intensity versus two theta angle) by the Matlab® routine. The diffraction peaks obtained were then analyzed using a single peak fitting routine available within GSAS/Rawplot® [26]. The peaks were fitted with a pseudo-Voigt function, which is a convolution of Gaussian and Lorentzian peak shapes. In the GSAS fitting routine the Lorentzian full-width at half maximum (FWHM) was kept constant, while the Gaussian full-width at half maximum was allowed to vary; the Lorentzian full-width at half maximum is normally associated with instrumental broadening (which was determined independently), whereas the Gaussian full-width at half maximum is normally associated with sample broadening, such as from size or strain broadening. The background was fit over the entire diffraction range using a third-degree polynomial function. The diffraction peaks were fit iteratively to obtain (i) the integrated intensity, (ii) the Gaussian full-width at half maximum (FWHM) and (iii) the peak positions of the refined peaks. When measured under stress, the shift in peak position can be related to the elastic strain of the diffracting crystallites (or change in stoichiometry), while peak broadening can originate from various causes,
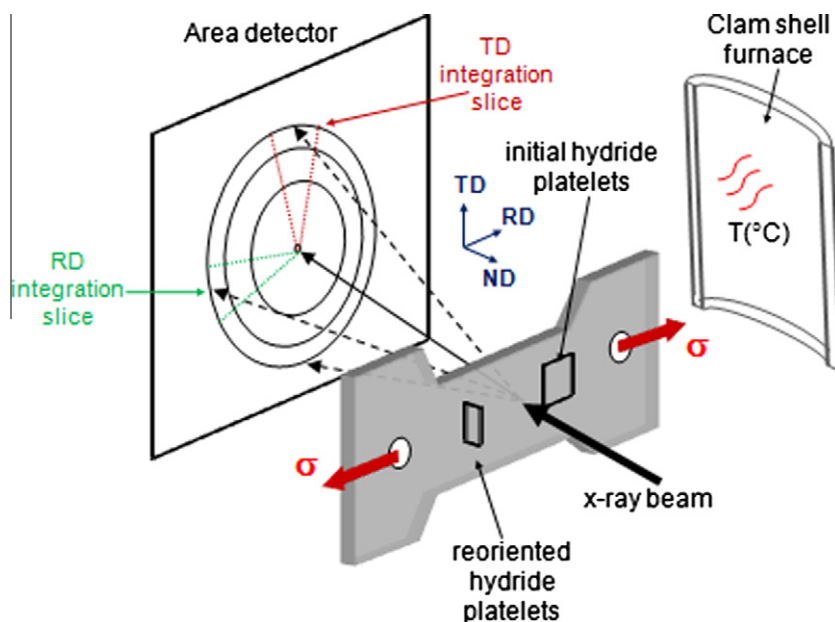

Fig. 3. Experimental set-up for hydride re-orientation experiments at beamline 1-ID at the APS.
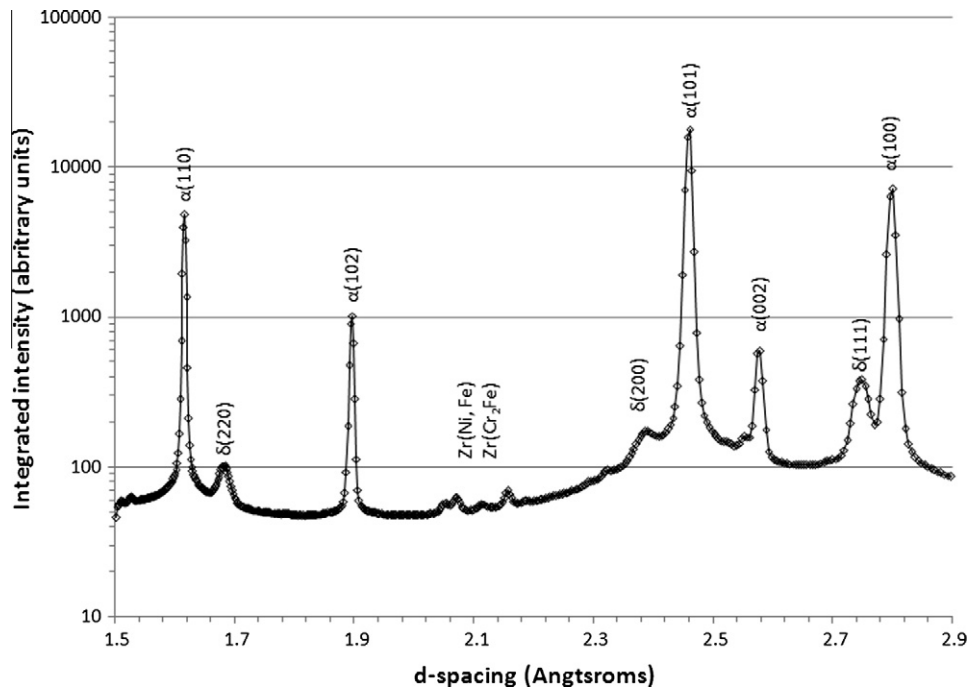
Fig. 4. Diffracted intensity versus d-spacing, obtained for the integration over the entire diffraction ring for a Zircaloy-2 sample with 600 wt. ppm of hydrogen (logarithmic scale).

including size broadening, inhomogeneous elastic strain and plastic strain broadening [27].

3. Results and discussion

3.1. Kinetics of hydride dissolution and precipitation

The determination of the dissolution and precipitation temperatures was performed by studying the diffraction signal from the zirconium hydrides. As the sample is heated and the hydrides dissolve, the diffraction peak intensity from the hydride decreases. This is illustrated in Fig. 5 where the integrated intensity for the $(1\,1\,1)_\delta$ hydride peak is plotted as a function of time for two samples. For sake of clarity, only the RD integration range is plotted in the figure; the data obtained for the TD integration range is very similar; the integration range seems to have little effect in the measured dissolution and precipitation kinetics.

The temperature during the heating cycle is shown on the right-hand axis. The diffraction signals of the $(1\,1\,1)_\delta$ peaks measured in two samples (containing 530 and 110 wt. ppm H) are both shown in this figure. It is clear that the hydride peak diffracted intensity from the sample containing 530 wt. ppm of hydrogen is higher than that from the sample containing 110 wt. ppm of hydrogen. When the temperature (and thus the hydrogen solubility) is increased the hydrides begin to dissolve, and their diffracted intensity decreases until at the dissolution temperature the peaks disappear. When the temperature decreases from the maximum, hydrides precipitate from solid solution causing the hydride diffracted intensity to increase.

This data can be used to determine when the hydrides dissolve and precipitate and the corresponding dissolution and precipitation temperatures. The dissolution temperature, T_d, is defined as the temperature at which the diffracted intensity reaches zero upon heating (all the hydrides have dissolved) and the precipitation temperature, T_p, is the last temperature at zero intensity (i.e. no hydrides have yet precipitated) upon cooling. The measured dissolution and precipitation temperatures determined in samples with various hydrogen contents are shown in Fig. 6. In this figure, the T_d and T_p for each sample are compared to T_d and T_p curves determined in Une and Ishimoto [28] using differential scanning calorimetry (DSC). From Fig. 6 it is seen that the measured T_d and T_p for all samples correspond reasonably well to the temperatures measured in [28]. The magnitude of the hysteresis observed between T_d and T_p is also similar to that observed using DSC in [28]. Comparison between diffracted intensity from X-ray diffraction and DSC is justified by the fact that both techniques have measured hydrogen dissolution and precipitation for samples containing down to 20 wt.ppm of hydrogen [4,29]. It is thus expected that these techniques can be compared fairly well.

3.2. Effect of heating and cooling rates on dissolution and precipitation temperatures

This technique also allows the study of the effect of heating and cooling rates on the dissolution and precipitation temperatures. A sample containing 80 wt.ppm of hydrogen was submitted to three consecutive cycles of going to
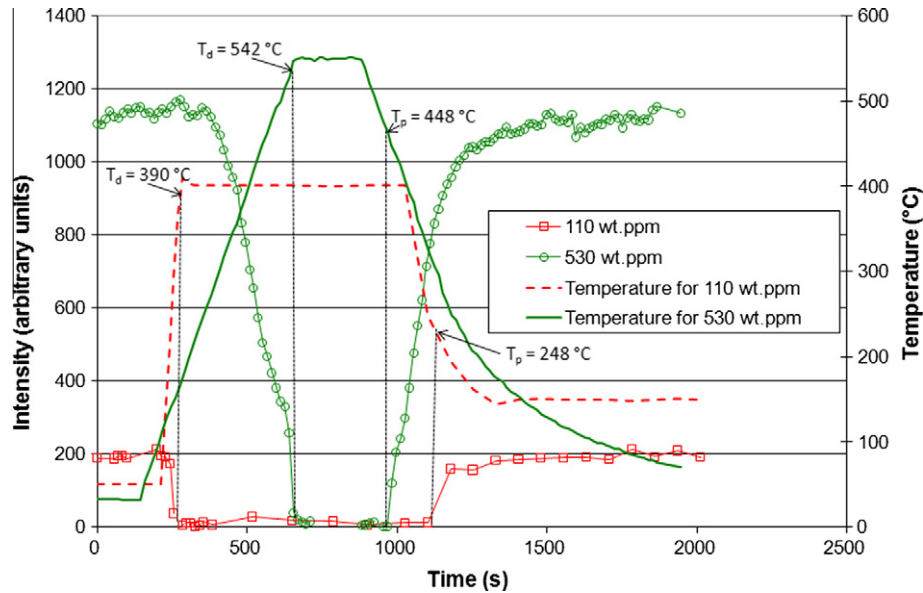
Fig. 5. Evolution of the integrated intensity of delta (1 1 1) hydride peaks from the RD angular range with temperature for two temperature cycles performed on Zircaloy-2 ND samples with 110 wt. ppm and 530 wt. ppm of hydrogen with no applied load.
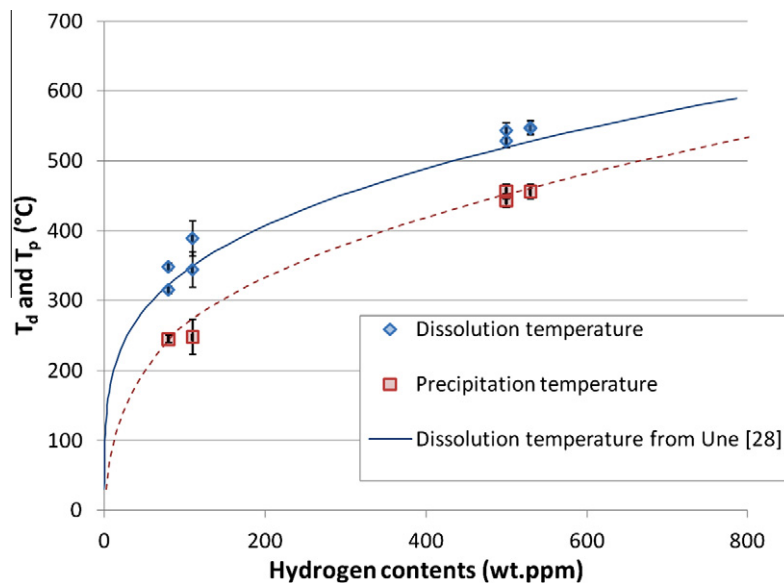

Fig. 6. Hydrogen dissolution and precipitation temperatures in Zircaloy-2 as a function of hydrogen content, as compared to values for [28].

400 °C, holding for 5 min and cooling. In each case, the dissolution and precipitation temperatures were determined as in the preceding section. The heating rate varied from 5 °C/s to 0.05 °C/s while the cooling rate varied from 1 °C/s to 0.05 °C/s. Little effect was seen of the heating rate on the dissolution temperature and the values corresponded as above with those measured by DSC. A small decrease was observed in the precipitation temperature at high cooling rates.

We should note that the different cooling rates were obtained for consecutive thermal cycles. Measurements in later cycles, as is well known, can be affected by a 'memory effect' on hydride precipitation [30]. Thus, although mea-

surements should be considered preliminary, the more pronounced effect of cooling rate on T_p than heating rate on T_d is consistent with previous work from Pan et al. [31].

3.3. Hydride re-orientation and estimation of threshold stress for re-orientation

A second series of experiments was carried out in which a uniaxial load was applied to the sample during cool down. The objective of these experiments was to study the effect of applied load on hydride dissolution and precipitation, including dissolution and precipitation temperatures, and possible re-orientation of hydrides upon re-
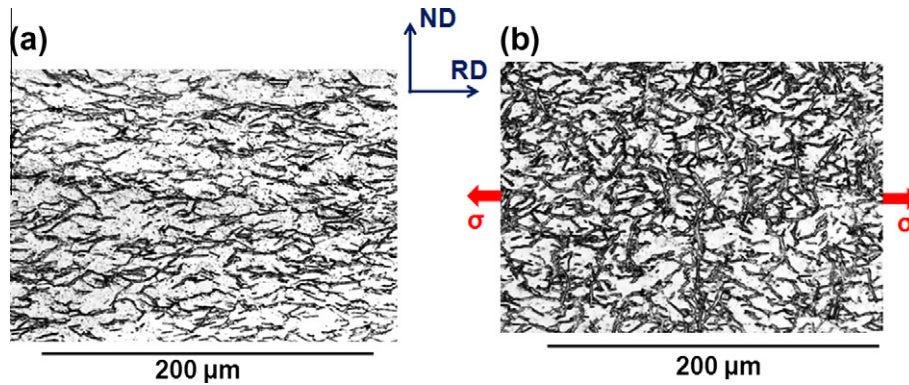
Fig. 7. Optical metallography of hydride orientation before and after cooling under load (a) Zircaloy-4 sample with 608 wt. ppm of hydrogen and (b) same sample after being heated up to 500 °C then cooled down with an applied tensile stress of 85 MPa (indicated).

precipitation. To determine the threshold stress for hydride re-orientation, metallography was performed on samples prior to and after the heat/load cycle. The radial hydride content was estimated using image analysis. Fig. 7 shows metallographs of a Zircaloy-4 sample with 608 wt. ppm of hydrogen before (7(a)) and after (7(b)) the last heating/cooling cycle under load. Initially, in Fig. 7a, the hydride platelets are perpendicular to the ND and thus they are in-plane or 'circumferential hydrides'. After re-orientation, in Fig. 7b, some hydride platelets, have reoriented perpendicular to the tensile direction (RD). To determine the radial hydride content of a sample, each individual particle was counted as either a circumferential hydride, a mixed hydride or a radial hydride. The circumferential hydrides were those whose normals were oriented between 0° and 40° from the normal direction (or radial direction for a cladding tube), the mixed hydrides were those whose normals were oriented between 40° and 65° from the normal direction and the radial hydrides were those whose normals were oriented between 65° and 90° from the normal direction. The radial hydride content in per cent was defined as:

$$RHC = 100 \times (0.5 \times N_{MH} + N_{RH})/N_{TOTAL} \qquad (1)$$

where the RHC is the radial hydride content in per cent, the N_{MH} is the number of mixed hydrides, N_{RH} is the number of radial hydrides and N_{TOTAL} is the total number of hydrides. According to this definition the RHC of the hydrided cladding shown in Fig. 7a was 15% while that of 7(b) was 33%. The radial hydride content increases after the heat/cool cycles if the applied load causes a high enough stress. Fig. 8 shows the variation of the RHC with applied tensile stress for Zircaloy-2 and Zircaloy-4 samples with approximately 600 wt. ppm of hydrogen. The initial RHC for all samples was between 15 and 20% as represented by the value at zero load. For the Zircaloy-2 samples, the per cent of radial hydrides after cooling under a stress of 75 MPa was about 40%, compared to initial values of about 20%. The fact that no meaningful difference in RHC is seen between the Zircaloy-2 samples cooled at stresses from 75 to 100 MPa (significant RHC increase is

seen in both) suggests that the threshold stress is lower than 75 MPa. For the Zircaloy-4 sample, a clear increase is observed of the RHC after a temperature cycle at about 85 MPa and no increase is seen after a temperature cycle at 75 MPa, which suggests that the threshold stress for re-orientation in this Zircaloy-4 is between those two values. However, it should be noted that for the Zircaloy-4 data point at 75 MPa load, 10% of the hydrides remained un-dissolved during the last heating/cooling under load cycle. This could cause the obtained RHC to be lower than expected for full dissolution of hydrides. Therefore the threshold stress for re-orientation of our Zircaloy-4 material could be lower than the 80 MPa that the data suggests.

The diffraction patterns from the reoriented hydrides exhibit a particular 'signature' when compared to those of non-reoriented hydrides. Specifically the hydride peak broadening reveals a particular behavior for reoriented hydrides. In Fig. 9, the Gaussian full-width at half maximum (FWHM) of the $(1\,1\,1)_\delta$ hydride peaks obtained from GSAS fits is plotted as a function of time during a thermal cycle under load. As in Fig. 5, the temperature cycle is
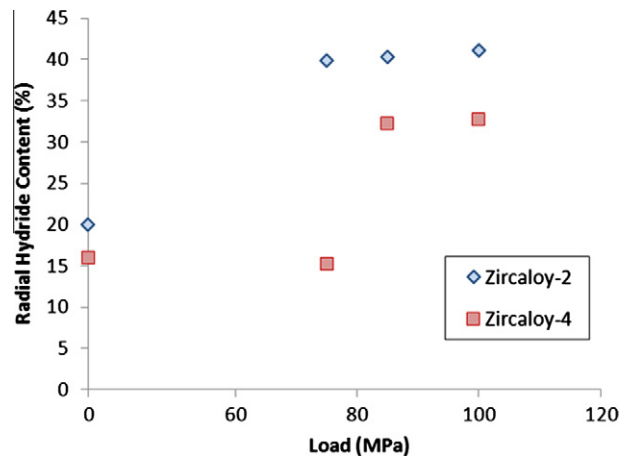

Fig. 8. Evolution of radial hydride content in per cent with tensile load applied to the sample for Zircaloy-2 and Zircaloy-4 samples which have approximately 600 wt. ppm.
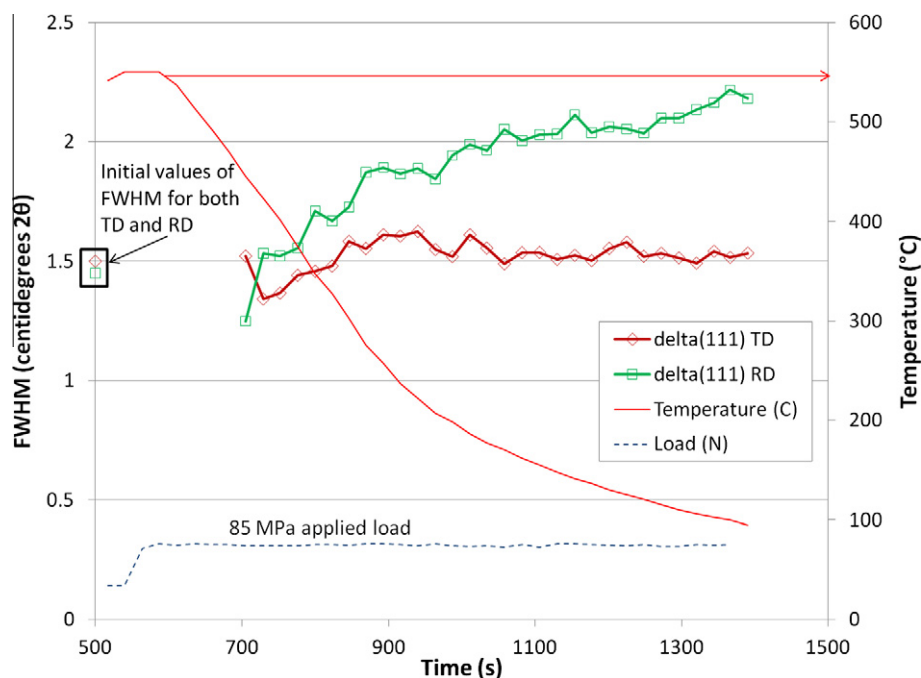
Fig. 9. Full-width at half maximum of the delta (1 1 1) hydride peaks of a Zircaloy-4 sample with 530 wt. ppm of hydrogen during the heat cycle shown. Sample was cooled under 85 MPa applied stress, resulting in hydride re-orientation.

represented by a solid line linked to the right-hand axis. Only the cooling side of the heat/cool cycle is shown. The load is applied in the RD when the temperature has reached a maximum and kept at a constant level upon cool down (load-controlled).

As the sample is cooled, the $(1\,1\,1)_\delta$ hydride peak intensity again increases, as was shown in Fig. 5. The full-width at half maximum of the hydride peaks is calculated from the diffraction pattern and compared to the value before the heat/cool cycle. When this comparison is performed for the sample cooled without applied stress, the full-width half maximum of the $(1\,1\,1)_\delta$ hydride peak returns to the value before the temperature cycle and remains constant thereafter. This is true for hydrides planes oriented in both TD and RD (data not shown due to space constraints). In contrast, for the samples cooled under load (Fig. 9) a marked difference is observed between the behavior of the full-width at half maximum of the delta (1 1 1) hydride peak for planes oriented in the TD and RD (the load is applied along RD). While the FWHM of the hydride planes whose normals are oriented along the direction perpendicular to the load (TD) behave in the same manner as those cooled under no stress,(returns to the previous value and remains constant), the FWHM of the delta (1 1 1) hydride planes whose normals are oriented parallel to the load show a different behavior. In this latter case the full-width at half maximum returns to the initial value upon initial precipitation and then continues to increase as the sample is cooled further. This behavior has been observed in both samples where hydride re-ori-

entation occurred (i.e. in the samples under 85 and 100 MPa stress) but not in samples in which hydrides did not reorient (in the sample cooled under 75 MPa stress or in the samples in which no load was applied).

It should be noted that the zirconium peaks have also been fitted and monitored during the in situ experiment. Within experimental uncertainty, the positions of the zirconium peaks followed the expected behavior from thermal expansion. After removing the load at the end of the experiment, the zirconium peak positions returned to their initial values, suggesting that no permanent deformation was observed in the zirconium. The zirconium peaks' integrated intensities and widths did not vary significantly under applied load during cool down. This suggests that the observed 'signature' for hydride re-orientation is due only to hydride behavior and that there is not a significant effect of zirconium matrix creep during the time of the experiment.

Peak broadening can result from strain broadening (both elastic strain and plastic strain), and from size broadening [27]. In this case, because the observed broadening increases as the hydrides grow (sample cools further) size broadening is ruled out as the main cause of the FWHM increase in the direction parallel to the load. The broadening then suggests that additional strain is incurred on the hydrides whose normals are oriented in the direction of the applied stress (the reoriented hydrides), as they grow relative to those who are not. It is not possible based on the data presented so far to determine whether such strain is elastic or plastic. Further work is required to resolve this question.

4. Conclusions

Detailed X-ray diffraction measurements were performed on various hydrided zirconium alloys samples using synchrotron radiation. The objective of the study was to validate the use of transmission diffraction experiments for in situ determination of the kinetics of dissolution and precipitation of zirconium hydrides as a function of applied load and temperature. The secondary objective of this study was to identify a diffraction "signature" associated with hydride re-orientation. Both in situ and ex-situ experiments were performed on samples of different orientations, under different levels of load, and the results were compared to metallographical examination. The dissolution and precipitation of hydrides was followed by recording the intensity of hydride diffraction peaks as the temperature was varied.

- The dissolution and precipitation temperature when heated and cooled under no applied stress were determined in situ for samples hydrided to various levels and under various cooling rates. The results were in good agreement with DSC literature values at slow cooling/heating rates.
- Upon application of stress during cooling from a temperature at which all hydrogen was dissolved, a fraction of the hydrides were found to reorient upon re-precipitation such that their habit planes were perpendicular to the applied stress direction. The degree of re-orientation was measured by the radial hydride content, which increased from 15 to 40% upon re-orientation. This re-orientation occurred for all samples at applied stresses above 80 MPa.
- A diffraction "signature" of reoriented hydrides was identified by studying the full-width at half maximum of the precipitated hydride peaks. The FWHM for the hydrides planes oriented perpendicular to the applied stress direction was found to increase after precipitation, while the FWHM of the hydrides planes oriented parallel to it did not. This signature was only observed in samples in which hydride re-orientation occurred.

Acknowledgements

References

[1] Daum RS. Hydride-induced embrittlement of Zircaloy-4 Cladding under plane-strain tension, PhD thesis in Materials Science. The Pennsylvania State University; 2007.
[2] Raynaud PAC. Crack growth through the thickness of thin-sheet hydrided Zircaloy-4, PhD thesis in Materials Science. The Pennsylvania State University; 2009.
[3] Daum RS, Chu YS, Motta AT. J Nucl Mater 2009;392:453.
[4] McMinn A, Darby EC, Schofield JS. Terminal solid solubility of hydrogen in zirconium alloys. In: Sabol GP, Moan GD, editors. Proc 12th Int Symp on Zirconium in the Nuclear Industry ASTM STP 1354: American Society for Testing and Materials; 2000. p. 173.
[5] Coleman CE, Hardie D. J Less Common Met 1966;11:168.
[6] Mardon JP, Lesbros A, Bernaudat C, Waeckel N. Recent data on M5(TM) alloy under RIA and LOCA conditions. In: Proc 2004 Int Meet LWR Fuel Perform; 2004. p. 507.
[7] Int Cent Diffr Data. The powder diffraction file; 2006.
[8] Bradbrook JS, Lorimer GW, Ridley N. J Nucl Mater 1972;42:142.
[9] Beck RL. Zirconium–hydrogen phase system. Trans ASM 1962;1:542.
[10] Perovic V, Weatherly GC, Simpson CJ. Acta Metall 1983;31:1381.
[11] Chung HM, Daum RS, Hiller JM, Billone MC. Characteristics of hydride precipitation in spent-fuel cladding. In: Moan GD, Rudling P, editors. Proc 13th Int Symp on Zirconium in the Nuclear Industry ASTM STP 1423: American Society for Testing and Materials; 2000. p.561.
[12] Ells CE. J Nucl Mater 1968;28:129.
[13] Kearns JJ, Woods CR. J Nucl Mater 1966;20:241.
[14] Singh RN, Kishore R, Singh SS, Sinha TK, Kashyap BP. J Nucl Mater 2004;325:26.
[15] Hardie D, Shanahan MW. J Nucl Mater 1975;55:1.
[16] Kammenzind BF, Berquist BM, Bajaj R, Kreyns PH, Franklin DG. The long-range migration of hydrogen through Zircaloy in response to tensile and compressive stress gradients. In: Sabol GP, Moan GD, editors. Proc 12th Int Symp on Zirconium in the Nuclear Industry ASTM STP 1354: American Society for Testing and Materials; 2000. p. 196.
[17] Kerr M, Daymond MR, Holt RA, Almer JD, Stafford S. Scr Mater 2010;62:341.
[18] Kerr M, Daymond MR, Holt RA, Almer JD, Stafford S, Colas KB. Scr Mater 2009;61:939.
[19] Root JH, Fong RWL. J Nucl Mater 1996;232:75.
[20] Root JH, Small WM, Khatamian D, Woo OT. Acta Mater 2003;51:2041.
[21] Xu F, Holt RA, Daymond MR, Rogge RB, Oliver EC. Mater Sci Eng: A 2008;473:139.
[22] Douglass DL. The Metallurgy of Zirconium. In: Turkov ZI, editor. Atomic Energy Review: Int Atomic Energy Agency, Vienna; 1971
[23] Pierron ON, Koss DA, Motta AT. J Nucl Mater 2003;312:257.
[24] Haeffner DR, Almer JD, Lienert U. Mater Sci Eng: A 2005;399:120.
[25] Almer JD, Lienert U, Peng RL, Schlauer C, Oden M. J Appl Phys 2003;94:697.
[26] Larson AC, Dreele RBV. General structure analysis system (GSAS). Los Alamos National Laboratory; 2000.
[27] Snyder RL, Fiala J, Bunge H. Defect and microstructure analysis by diffraction. International Union of Crystallography Monographs on Crystallography. Oxford: Oxford University Press; 1999.
[28] Une K, Ishimoto S. J Nucl Mater 2003;322:66.
[29] Vizcaino P, Banchik AD, Abriata JP. J Mater Sci 2007;42:6633.
[30] Northwood DO, Kosasih U. Int Met Rev 1983;28:92.
[31] Pan ZL, Ritchie IG, Puls MP. J Nucl Mater 1996;228:227.